ORIGINAL ARTICLE

Degradation of toxic methylene blue dye with Zinc oxide (ZnO) nanoparticles synthesized by leaf extract of *Madagascar periwinkle* plant

Akansha Gupta[1] · Sapna Yadav[2] · Nutan Rani[2] · Kalpna Gupta[3] · Kalawati Saini[2]

Abstract

In this paper, we have synthesized ZnO nanoparticles namely ZnO (L5) and ZnO (L10) nanoparticles. Both ZnO (L5) and ZnO (L10) nanoparticles have been synthesized by biosynthesis methods using *Madagascar periwinkle* leaf extract. The biosynthesis method is simple, eco-friendly, and cheap. ZnO (L5) and ZnO (10) nanoparticles have been characterized by using X-ray diffraction (XRD), Scanning Electron Microscopy (SEM), Energy Dispersive Spectroscopy (EDS), UV-Visible Spectroscopy, Fourier Transform Infrared Spectroscopy (FTIR), Field Emission Scanning Electron Microscopy (FESEM), Brunauer–Emmett–Teller (BET), and Transmission Electron Microscopy (TEM). The Powder X-ray diffraction (PXRD) revealed that synthesized ZnO (L5) and ZnO (L10) consist of a typical hexagonal wurtzite phase. The size and morphology of synthesized ZnO (L5) and ZnO (L10) nanoparticles were determined using Scanning Electron Microscopy (SEM), Field Emission Scanning Electron Microscopy (FESEM), and Transmission Electron Microscopy (TEM). The FTIR study reveals that phytochemicals from the leaf of the *Madagascar periwinkle* leaf extract are present on the surface of synthesized ZnO (L5) and ZnO (L10) nanoparticles. The BET analysis shows that the measured surface areas of ZnO (L5) and ZnO (L10) nanoparticles are 10.202 m^2/g and 38.762 m^2/g respectively. The photocatalytic activity of both the synthesized nanoparticles was determined against methylene blue (MB) organic dye. It was evident from the results that ZnO (L10) is a better catalyst than ZnO (L5). Herein, MB dye was degraded (94.09%) in 600 min by ZnO (L5) photocatalyst and (97.92%) in 360 min by ZnO (L10) photocatalyst. Therefore synthesized ZnO (L5) and ZnO (L10) nanoparticles could be employed as an efficient photocatalyst for the degradation of toxic organic dyes.

Keywords Biosynthesis · ZnO (L5) nanoparticles · ZnO (L10) nanoparticles · *Madagascar periwinkle* · Photocatalytic degradation · Organic dye

Abbreviations

XRD	X-Ray Diffraction
SEM	Scanning Electron Microscopy
EDS	Energy Dispersive Spectroscopy
UV	Ultraviolet
FTIR	Fourier Transform Infrared Spectroscopy
FESEM	Field Emission Scanning Electron Microscopy
BET	Brunauer-Emmett-Teller
TEM	Transmission Electron Microscopy
PXRD	Powder X-Ray Diffraction
MB	Methylene blue
LE	Leaf extract
AOPs	Advanced Oxidation Processes
NPs	Nanoparticles
rGO	Reduced graphene oxide
L5	ZnO nanoparticle synthesized using 5 mL of *Madagascar Periwinkle* plant's leaf extract
L10	ZnO nanoparticle synthesized using 5 mL of *Madagascar Periwinkle* plant's leaf extract

✉ Kalawati Saini
kalawati.saini@mirandahouse.ac.in

[1] Department of Chemistry, Gurugram University, Haryana 122003 Gurugram, India

[2] Department of Chemistry, Miranda House, University of Delhi, Patel Chest Marg, Delhi 110007, India

[3] Department of Chemistry, Raj Rishi Government College, Alwar 301001, Rajasthan, India

1 Introduction

Waste from various industrial and domestic sources contains organic chemicals in high concentration. This waste when discarded in natural water makes it hazardous and non-consumable. Approximately 30% – 40% of these organic chemicals are composed of organic dyes which are released from various textile industries [1]. Azo dyes are widely used in textile, paper, fruit, leather, cosmeceuticals, and pharmaceutical industries, making up the majority of dyestuffs produced [2]. These organic dyes are carcinogenic and have complex aromatic structures which makes them stable against natural degradation [3]. They are toxic if inhaled; absorbed or swallowed it may lead to multiple eyes, skin, and respiratory problems [4]. Therefore, researchers made several attempts to treat these problems [5].

Researchers used various biological treatments to remove these organic dyes from wastewater but it was ineffective such as the microorganisms present in water were not capable of degrading the organic dyes [6]. They used various physical methods like coagulation, oxidation or reduction, membrane filtration, sorption, chemical precipitation, photocatalysis, solvent extraction, and ion exchange to overcome these hazards [7]. Photocatalytic degradation is an important technique among them as it is economical, simple, safe, and efficient and it produces no secondary toxic byproduct [8, 9].

Flilissa et al. have used Bentonite/Sodium dodecylbenzene sulfonate composite for methylene blue removal from wastewater [10]. Utami et al. have synthesized N-TiO$_2$/rGO using the hydrothermal method for the removal of organic dye and heavy metal from textile wastewater [11]. Yadav et al. synthesized microcrystalline calcium carbonate particles using incense sticks ash and this synthesized microcrystalline calcium carbonate particles removed 48.6% of methyl red dye from the aqueous solution within one hour [12]. Naik et al. used a silica matrix as a substrate for zinc oxide nanoparticles (ZnO NPs) to increase their photocatalytic activity in the degradation of methylene blue (MB) dye [13].

Fetimi et al. have spent decades developing environmentally friendly advanced oxidation processes (AOPs) [14]. In recent times Advanced Oxidation Processes (AOPs) have also gained the attention of researchers for wastewater treatment as they involve the generation of free radicals [15]. Free radicals act as oxidizing agents and hence promote the oxidation of pollutants present in the water. It is a greener method used to convert the pollutants of wastewater into less toxic molecules [16].

Semiconductor-mediated photocatalysis is the most suitable method for the degradation of organic dyes [17].

They have low cost, high degradation efficiency, easy manipulation, broad usage, and relatively safer reaction conditions [18]. The basic principle of photocatalytic reaction involves the absorption of photons by a photocatalyst (semiconductor) which leads to the excitation of electrons from the valence band to the conduction band which creates electron deficiency or a hole in the valence band and generating electrons in the conducting band. The electron/hole moves towards the surface of the photocatalyst and undergoes a redox reaction thus generating radicals such as hydroxyl radicals which degrade the organic dyes [19].

Nanoparticles have been synthesized using wet chemical processes such as co-precipitation, microemulsion, chemical vapor deposition, hydrothermal, pyrolysis, radiation-induced, solvothermal, and electrodeposition. These procedures have several disadvantages, including the use of dangerous and harmful compounds, increased prices, ecotoxicity, high consumption levels, and by-products with longer reaction times [20]. Plants are a natural source of different biologically active chemicals [21]. Biological synthesis is a cost-effective and ecologically benign approach to producing nanoparticles. It employs biological reducing and stabilizing agents, as well as catalysts [22]. Bhusal et al. have synthesized trimetallic Cu/Fe/Zn nanoparticles (NPs) by using *Catharanthus roseus* leaf extract [23]. Idris et al. fabricated Silver–Zinc bimetallic nanoparticles using *Actinidia chinensis var. deliciosa* (Kiwi) peel extract [24].

Semiconductors of various metal oxides such as TiO$_2$, Fe$_2$O$_3$, CdS, ZnO, V$_2$O$_5$, NiO, etc. were used as photocatalysts for the degradation of organic dyes [9, 19, 25, 26]. Zinc oxide (ZnO) has been used mainly due to its great intrinsic properties and high environmental remediation [27]. ZnO has low cost, high biocompatibility, excellent chemical stability, and a unique structure [28]. However, its application is inhibited due to broadband gap and recombination of photons with high speed [29]. Zinc oxide (ZnO) is a semiconductor with a direct band gap of 3.37 eV and a high exciton binding energy of 60 mV at 300 K. Zinc oxides are nearly insoluble in water. It is also optically clear within the visible spectrum. We can overcome this by doping of ZnO structure with the help of metals or non-metals or by the formation of heterojunction with any other semiconductor [30]. Modi et al. have reported the ZnO nanoparticles in the remediation of MB dye from wastewater [31].

In this research article, we have reported *Madagascar periwinkle* leaf extract mediated green synthesis of ZnO NPs and evaluated their potential as the photocatalyst. Phytochemicals found in leaves play a significant role in the synthesis of nanoparticles and affect the degradation of dyes. Catharanthus roseus, also known as the Madagascar periwinkle, is a native plant of Madagascar. The extract of its leaves contains various phytochemicals, mainly alkaloids such as Vincristine, Vinblastine, Vinpocetine, Reserpine,

Ajmalicine, Ajmaline, Yohimbine, Vindolidine, Catharan-thine, Vindoline, Serpentine, Vindesine, Vindolicine, and Vindolinine, which contain different functional groups [32]. These functional groups on the surface of synthesized ZnO (L5) and ZnO (L10) nanoparticles play a crucial role in the adsorption of dye molecules on their active sites. When more dye molecules are adsorbed on the active sites of synthesized photocatalysts, it leads to multilayer adsorption, which follows the Brunauer–Emmett–Teller (BET) isotherm. Therefore, the rate of degradation of MB dye molecules becomes high which leads to a decrease in the time of degradation.

2 Experimentation

2.1 Materials

Zinc acetate [Zn $(COOCH_3)_2$] (pure minimum assay, 99.0%), sodium hydroxide [NaOH] (minimum assay, 97.0%), ethanol [C_2H_5OH] (pure minimum assay, 99.9%), and methylene Blue (MB) (pure minimum assay, 96.0%) were purchased from Central Drug House (P) Ltd, India. The chemicals were used without further purification. All the experiments were performed in double distilled water.

2.2 Collection of plant's leaves

Fresh healthy leaves of *Madagascar periwinkle* plant (Sada-bahar) were collected from the garden of Miranda House, Delhi University.

2.3 Preparation of 10% Leaf Extracts (LE)

The collected *Madagascar periwinkle* plant's leaves were further washed thoroughly and then blotted using a blotting paper. After that, they were kept for drying in an oven at 80 °C for 3 h and were crushed manually.

The dried and powdered leaves of amount 3.0 g were taken in a beaker of 100 mL, after that 30 mL of distilled water was added and kept on a hotplate magnetic stirrer (at 500 rpm) for 30 min at 40 °C. The freshly prepared leaf extract (LE) was filtered using Whatman filter paper.

2.4 Synthesis of Zinc oxide [ZnO] nanoparticles

Two sets of experiments were set up in order to synthesize ZnO nanoparticles (L5 and L10). In the first set 50 mL of 0.5 M [Zn$(COOCH_3)_2$] and 5 mL of *Madagascar periwinkle* leaf extract were taken in one beaker. This reaction solution was kept on hotplate magnetic stirrer for 5 min. After 5 min 50 mL of 0.5 M NaOH solution were added to precursor solution. The reaction solution was allowed to heat at 40 °C with constant stirring for 2 h. After 2 h, a white-colored

colloidal solution obtained was washed using 50% ethanol solution several times and dried at 80 °C for 4 h in a hot air oven. Dried powders were then placed in a furnace for calcination at 700 °C for 8 h to get ZnO (L5) nanoparticles.

Similar process was performed for the synthesis of ZnO (L10) nanoparticles by using 10 mL of *Madagascar periwinkle* leaf extract instead of 5 mL leaf extract.

2.5 Characterization

The crystalline nature of both ZnO (L5) and ZnO (L10) nanoparticles formed was analyzed using the X-ray diffraction technique [D8 Discover X-ray diffractometer (Brucker equipped with Cu Kα) with X-ray source having a wavelength of 1.5406 Å. The morphology and the size of ZnO (L5) and ZnO (L10) nanoparticles were determined using Scanning Electron Microscope (SEM –JEOL, JAPAN: Model No.: JSM-6610LV), Field emission scanning electron microscope (FESEM, JEOL JSM7600 plus), and Transmission electron microscope (TEM) (JEOL, JEM – 2100 Plus electron microscope). The elemental composition of zinc oxide nanoparticles was analyzed using inbuilt energy dispersive X-ray spectroscopy (EDS). The optical properties of synthesized nanoparticles were analyzed through UV–visible spectroscopy (Spectramax M2e UV–visible spectrophotometer). Composition and functional groups of both the nanoparticles were analyzed through Fourier transform infrared spectroscopy (FTIR) through Perkin Elmer (Model No.: SPECTRUM RXI-MID IR, IR range of 400 to 4000 cm^{-1} having a resolution of 1 cm^{-1}). Surface area was observed by Brunauer–Emmett–Teller (BET) (St 1 on NOVA touch 2LX [s/n:17018101201]). Nitrogen (N_2) gas was used as adsorbate and the range of relative pressure (P/P_0) was 0.01–0.99.

2.6 Photocatalytic behavior study of ZnO (L5) and ZnO (L10) nanoparticles

Two different sets of experiments were set up in order to study the photocatalytic behavior of ZnO (L5) and ZnO (L10) catalysts against Methylene Blue (MB) dye. 50 mL of 10 ppm MB dye solution was prepared as a test solution for each experiment. Initially, we kept the MB dye in sunlight just to observe the photocatalytic degradation in the absence of a catalyst. Then we treated the MB dye with 50 mg of ZnO (L5) photocatalyst in one experiment and 50 mg of ZnO (L10) photocatalyst in another. Both chemical reactions were stirred using a magnetic stirrer for 30 min in the dark at room temperature before proceeding to the MB dye degradation process in order to maintain the absorption desorption equilibrium. The chemical reactions were then kept under intense sunlight so MB dye degradation could begin.

3 Result and discussion

3.1 Powder X-Ray Diffraction (PXRD)

The Powder X-Ray Diffraction (PXRD) determined the size of the crystallites and the crystalline nature of the synthesized ZnO (L5) nanoparticles and ZnO (L10) nanoparticles. The PXRD patterns of the synthesized ZnO (L5) and ZnO (L10) nanoparticles have been shown in Fig. 1(A) and Fig. 1(B) respectively. As shown in Fig. 1(A) ZnO (L5) exhibits peaks at 2θ values of 31.76°, 34.32°, 36.32°, 47.72°, 56.60°, 63.12°, 66.40°, 67.88°and 69.22° which were corresponding with (100), (002), (101), (102), (110), (103), (200), (112) and (201) hkl values respectively. Similarly, Fig. 1(B) exhibits peaks at 2θ values of 31.74°, 34.58°, 36.32°, 47.48°, 56.80°, 62.92°,66.66°, 68.04° and 69.16° which were corresponding with (100), (002), (101), (102), (110), (103), (200), (112) and (201) hkl values respectively.

PXRD patterns confirm that synthesized ZnO (L5) and ZnO (L10) nanoparticles consist of a typical hexagonal wurtzite phase (JCPDS card no. 36–1451) [33]. The crystallite sizes of the synthesized ZnO nano-photocatalysts were calculated using the Scherrer equation (Eq. 1). The Scherrer equation is reported in the literature [34] which is given as follows.

$$D = \frac{k\lambda}{\beta cos\theta} \tag{1}$$

where D is the crystallite size of synthesized material, k is the Scherrer constant (0.9), λ is the X-ray wavelength (0.154 nm), β is the full width at the half maximum intensity of diffraction peak (FWHM), and θ is the Bragg angle of diffraction peak. The calculated average crystallite size

of the ZnO (L5) and ZnO (L10) nanoparticles is 23.13 nm and 21.89 nm respectively.

3.2 Scanning Electron Microscopy (SEM), Field emission scanning electron microscopy (FESEM), Transmission electron microscopy (TEM), and Energy Dispersive X-Ray Analysis (EDS)

The size and morphology of synthesized ZnO (L5) and ZnO (L10) nanoparticles were determined using Scanning Electron Microscope (SEM), Field emission scanning electron microscope (FESEM), Transmission electron microscopy (TEM). The SEM, FESEM, and TEM images of ZnO (L5) and ZnO (L10) nanoparticles have been given in Fig. 2. ZnO (L5) nanoparticles are composed of rough surface with micro sized pores along with nanoflakes, and micro flakes. Dimensions of nanoflakes vary from ~ 100 nm to ~ 400 nm. Whereas, ZnO (L10) nanoparticles are composed of nanorods and nanoflakes. The length of nanorods ranges from ~ 50 nm to ~ 60 nm while the width of nanorods ranges from ~ 20 nm to ~ 50 nm. Dimensions of nanoflakes vary from ~ 50 nm to ~ 100 nm. It is clearly visible from FESEM and TEM images that size of ZnO (L10) nanoparticles is smaller than the size of ZnO (L5) nanoparticles.

The elemental composition of ZnO (L5) and ZnO (L10) nanoparticles was analyzed through EDS spectra. Figure 3(A) and Fig. 3(B) clearly shows the peaks of zinc and oxygen this indicates that zinc oxide nanoparticles were synthesized successfully. The peaks of zinc and oxygen only further confirm the presence of these elements in the nanoparticles. The atomic % ratios of Zinc and Oxygen were obtained at 28.93% and 71.07% respectively for ZnO (L5) nanoparticles as shown in Table 1. In ZnO (L10)
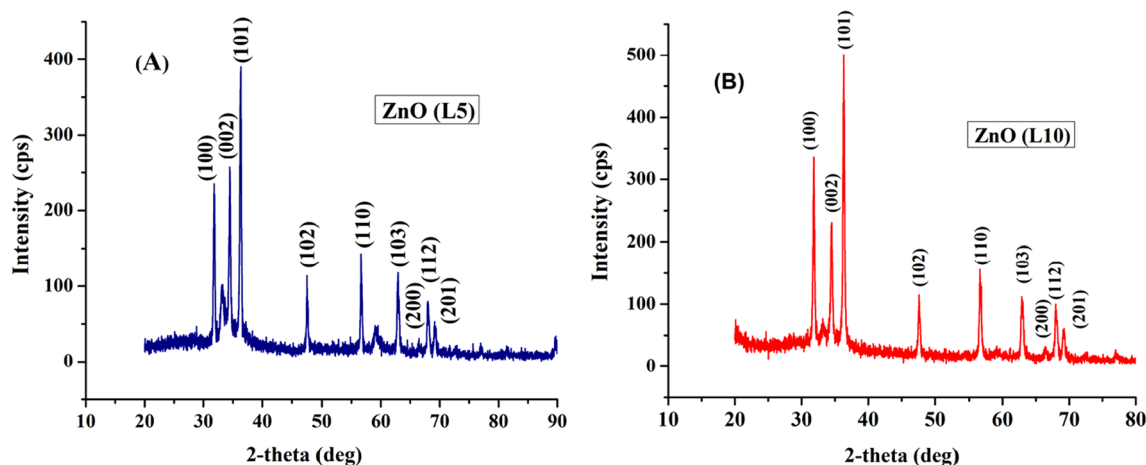

Fig. 1 (**A**) and (**B**) PXRD patterns of synthesized ZnO (L5) and ZnO (L10) nanoparticles
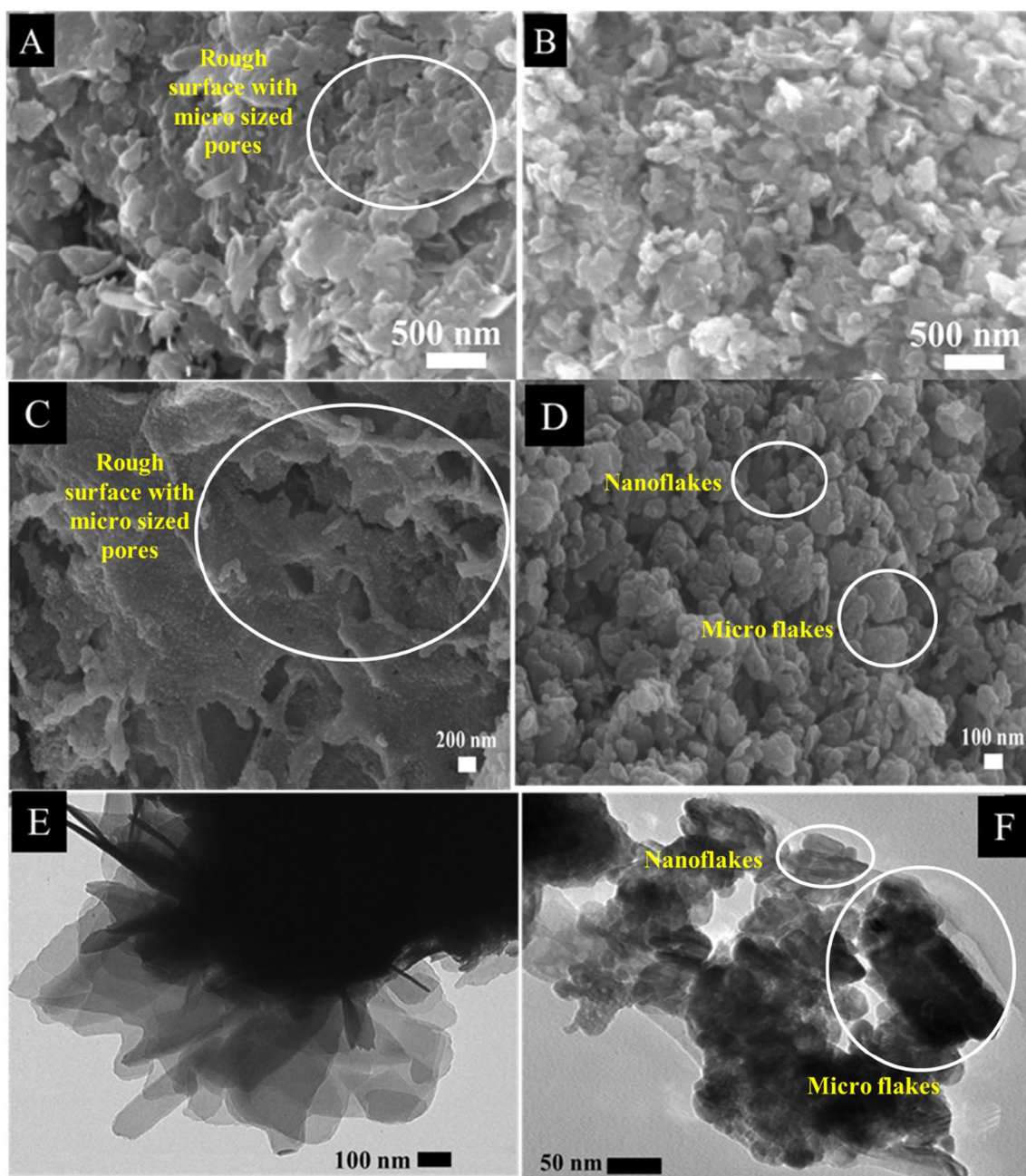
Fig. 2 (**A**) SEM images of synthesized ZnO (L5) nanoparticles, (**B**) SEM images of synthesized ZnO (L10) nanoparticles, (**C**) FESEM images of synthesized ZnO (L5) nanoparticles, (**D**) FESEM images of synthesized ZnO (L10) nanoparticles, (**E**) TEM images of synthesized ZnO (L5) nanoparticles, (**F**) TEM images of synthesized ZnO (L10) nanoparticles

nanoparticles, the atomic % ratios of Zinc and Oxygen were 41.49% and 58.51% respectively as shown in Table 2.

3.3 UV- visible spectrum analysis

The band gaps and optical properties of synthesized ZnO (L5) and ZnO (L10) nanoparticles are investigated through UV- Visible spectrum analysis. Figure 4(A) and Fig. 4(B) shows the UV- Visible spectrum of synthesized ZnO (L5)

and ZnO (L10) nanoparticles respectively. The maximum absorption is observed at a wavelength of 370 nm. This indicates that our ZnO (L5) and ZnO (L10) nanoparticles were synthesized successfully. Su et al. and Li et al. have reported similar absorption maxima (λ_{max}) for ZnO nanoparticles [35, 36].

We use Tauc's equation in order to examine the direct band gap of synthesized ZnO nanoparticles. Tauc's equation has been mentioned in the literature [9, 37, 38].

Fig.3 EDS analysis of synthesized (**A**) ZnO (L5) nanoparticles and (**B**) ZnO (L10) nanoparticles
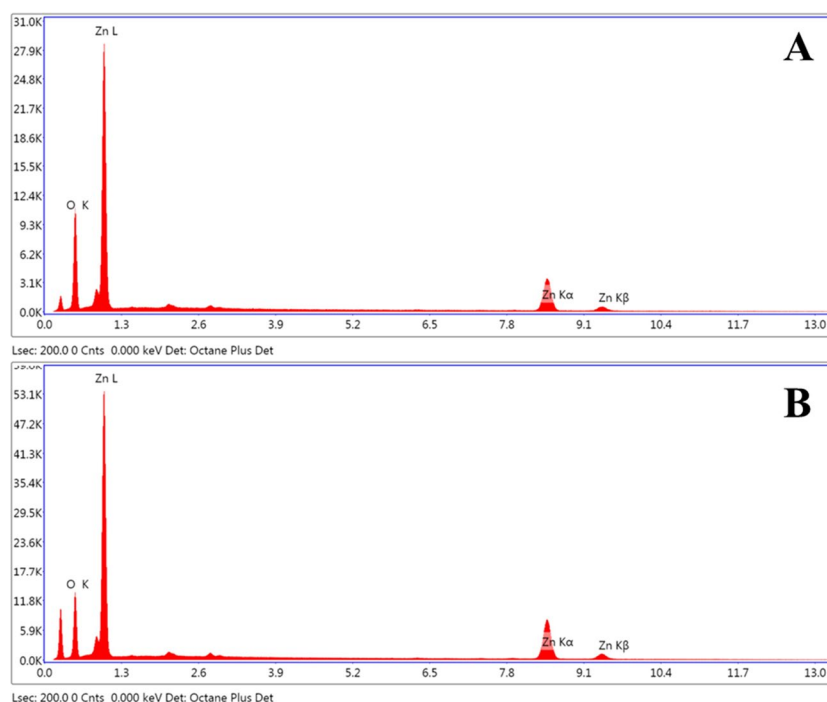

Table 1 Energy Dispersive X-Ray Analysis (EDS) for ZnO (L5) nanoparticles

Element	Weight %	Atomic %	Net Int	Error %
O K	37.54	71.07	351.06	7.52
Zn K	62.46	28.93	279.68	2.43

Table 2 Energy Dispersive X-Ray Analysis (EDS) for ZnO (L10) nanoparticles

Element	Weight %	Atomic %	Net Int	Error %
O K	25.66	58.51	400.64	7.96
Zn K	74.34	41.49	630.12	2.15

$$(a h\upsilon)^{\frac{1}{\gamma}} = A\left(h\upsilon - E_g\right) \tag{2}$$

where hυ is the energy of the photon, A is constant, E_g is band gap energy and γ is 2 for indirect allowed transition and ½ for direct allowed transition. The Tauc's plot $(a h\upsilon)^2$ v/s hυ of ZnO (L5) and ZnO (L10) nanoparticles have been shown in Fig. 4(C) and Fig. 4(D) respectively. The band gap value of ZnO (L5) nanoparticles was found to be 2.71 eV while the band gap value of ZnO (L10) was found to be 3.40 eV. The band gap value of ZnO (L5) and ZnO (L10) are in good agreement with the literature. Rahman et al. have reported the band gap energy of value 3.29 eV for the synthesized ZnO nanoparticle in the literature [34]. The band gap energy value of ZnO (L10) was found to be greater than ZnO (L5) this indicates that ZnO (L5) is a better semiconductor.

3.4 Fourier Transform Infrared Spectroscopy Analysis (FTIR)

The functional group analysis was done using FTIR. It helped us to determine the presence of functional groups on the surface of the synthesized nanoparticles. The FTIR spectra of zinc oxide nanoparticles range from 400 cm^{-1} to 4000 cm^{-1}.

In FTIR analysis of ZnO (L5), as shown in Fig. 5(A), the peaks observed between 578 cm^{-1} and 640 cm^{-1} occur due to the presence of vibrations of metal–oxygen bonds. The peaks at 986 cm^{-1} and 1173 cm^{-1} occur due to the presence of an alkene group on the synthesized nanoparticles. The peak at 1483 cm^{-1} is due to the carboxylic acid group [36]. The peaks at 1545 cm^{-1}—1688 cm^{-1} and 3367 cm^{-1}—3899 cm^{-1} are due to the presence of water or the OH group on the surface [9, 33, 38].

Similarly in FTIR analysis of ZnO (L10) as shown in Fig. 5(B), peaks at 586 cm^{-1} – 684 cm^{-1} occurs due to the presence of metal–oxygen bond vibrations. The peaks at 977 cm^{-1} -1181 cm^{-1} are due to the presence of an alkene group on the surface. The peak at 1475 cm^{-1} is due to the carboxylic acid group [36]. The peaks at 1590 cm^{-1} to 1732 cm^{-1} and 3411 cm^{-1} to 3491 cm^{-1} is due to the presence of water or the OH group on the surface of synthesized nanoparticles [9, 33, 38].

Fig. 4 UV- Visible Spectra of (**A**) ZnO (L5) and (**B**) ZnO (L10) nanoparticles and Tauc's plot of (**C**) ZnO (L5) and (**D**) ZnO (L10) nanoparticles
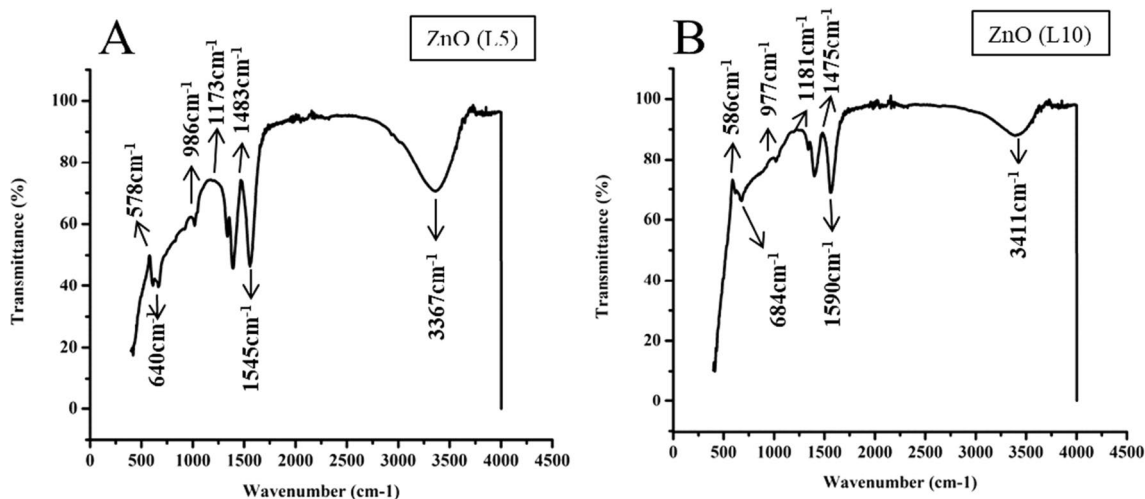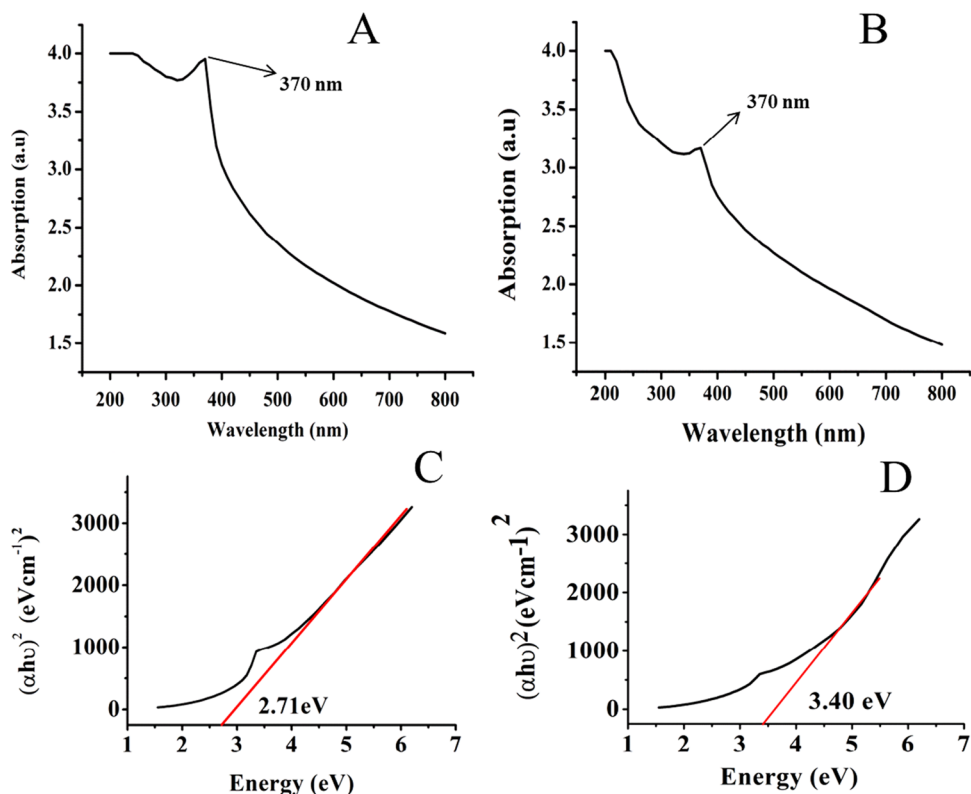

Fig.5 FTIR spectroscopy of synthesized (**A**) ZnO (L5) and (**B**) ZnO (L10) nanoparticles

The FTIR study reveals that phytochemicals from the leaf of the *Madagascar periwinkle* plant are present on the surface of synthesized ZnO (L5) and ZnO (L10) nanoparticles. This further confirms that leaves of the *Madagascar periwinkle* plant act as a good stabilizing agent in the synthesis of ZnO nanoparticles.

3.5 Brunauer–Emmett–Teller (BET) surface analysis

The N_2 adsorption/desorption (BET) isotherms of the synthesized ZnO (L5) and ZnO (L10) nanoparticles are shown in Fig. 6. Both ZnO (L5) and ZnO (L10) nanoparticles exhibit type IV adsorption/desorption isotherms according
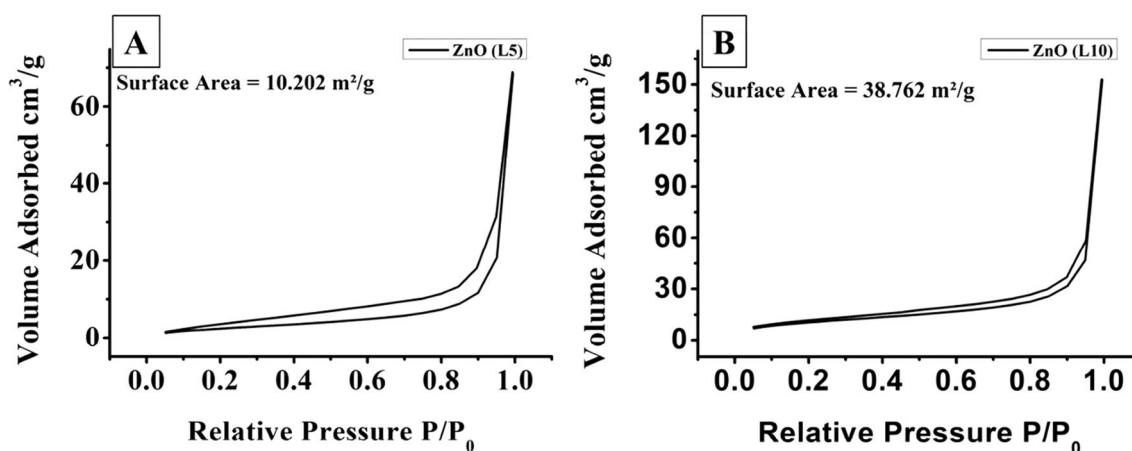
Fig. 6 N_2 adsorption/desorption isotherms of synthesized (**A**) ZnO (L5) nanoparticles and (**B**) ZnO (L10) nanoparticles

to the IUPAC classification [39], with a type H3 adsorption/desorption hysteresis loop. The existence of H3 adsorption/desorption hysteresis loops in ZnO (L5) and ZnO (L10) nanoparticles demonstrates their mesoporous nature [39]. The measured surface areas of ZnO (L5) and ZnO (L10) nanoparticles are 10.202 m^2/g and 38.762 m^2/g respectively. The findings of BET surface study show that ZnO (L10) nanoparticles have a larger surface area than ZnO (L5) nanoparticles. Thus, ZnO (L10) nanoparticles are a better photocatalyst for degradation MB dye than ZnO (L5) nanoparticles. Similarly, the surface area of 22.721 m^2/g has been calculated for ZnO (P3) nanoparticles [40].

3.6 Evaluation of photocatalytic activity of synthesized nanoparticles against Methylene Blue (MB) dye

We took 50 mL of 10 ppm MB dye solution as a test solution and added 50 mg of ZnO (L5) catalyst into it and kept it for 30 min. We observed there was no dye degradation (As shown in Fig. 7(A)). Then we kept this reaction mixture in sunlight for 30 min still no dye degradation was observed (As shown in Fig. 7(A)). We kept the reaction mixture in sunlight for 600 min and observed the photocatalytic activity of ZnO (L5) using UV spectrophotometry. As shown in Fig. 7(B) a graph between absorbance and wavelength (λ_{max} (nm)) was plotted where the reaction mixture was kept under different time intervals of sunlight irradiation. It is clear from Fig. 7(B) that as the time of sunlight irradiation increases, the dye degradation also increases. At 600 min the dye was degraded completely.

The same procedure was followed using ZnO (L10) catalyst. No dye degradation was found when we kept the reaction mixture for 30 min in the dark or even in the presence of sunlight as shown in Fig. 7(C). As shown in Fig. 7(D) a graph was plotted between absorbance and wavelength

(nm) where we checked the photocatalytic activity of ZnO (L10) in the presence of different sunlight irradiation. It was observed that as the time of sunlight irradiation increases, the dye degradation also increases. The dye degrades completely in 360 min in the presence of a ZnO (L10) catalyst.

Figure 7(A) and Fig. 7(C) indicates a decrease in absorption maxima with respect to sunlight irradiation time. This is the evidence for the degradation of toxic MB dye in the presence of ZnO nanoparticle photocatalysts. The Beer-Lambert Law suggests that the reduction in the absorption maxima means the reduction in the concentration of dyes with sunlight irradiation time [41].

After that photocatalytic degradation efficiency was calculated using the following formula which is given in the literature [9].

$$E\% = \left[\frac{C_0 - C_t}{C_0}\right] \times 100 \tag{3}$$

where C_0 is the initial concentration and C_t is the concentration of MB at different time intervals of the photocatalytic reaction. For ZnO (L5) catalyst, the photocatalytic degradation efficiency was found to be 19.59% at 60 min and 94.09% at 600 min. For ZnO (L10) catalyst it was observed to be 41.07% at 60 min and 97.92% at 360 min. After that a graph was plotted between ln (C_0/C_t) and time (in min) as shown in Fig. 7(E) in order to compare the photocatalytic degradation efficiency for ZnO (L5) and ZnO (L10) catalyst. It is evident from Fig. 7(E) that ZnO (L10) is a better catalyst than ZnO (L5). Herein, MB dye was degraded (94.09%) in 600 min by ZnO (L5) catalyst and (97.92%) in 360 min by ZnO (L10). Comparison of present study with earlier reported studies has been shown in Table 3.

Ulla and Dutta have reported the enhanced photocatalytic activity for the degradation of organic dyes of Mn-doped ZnO nanoparticles. They have reported that a
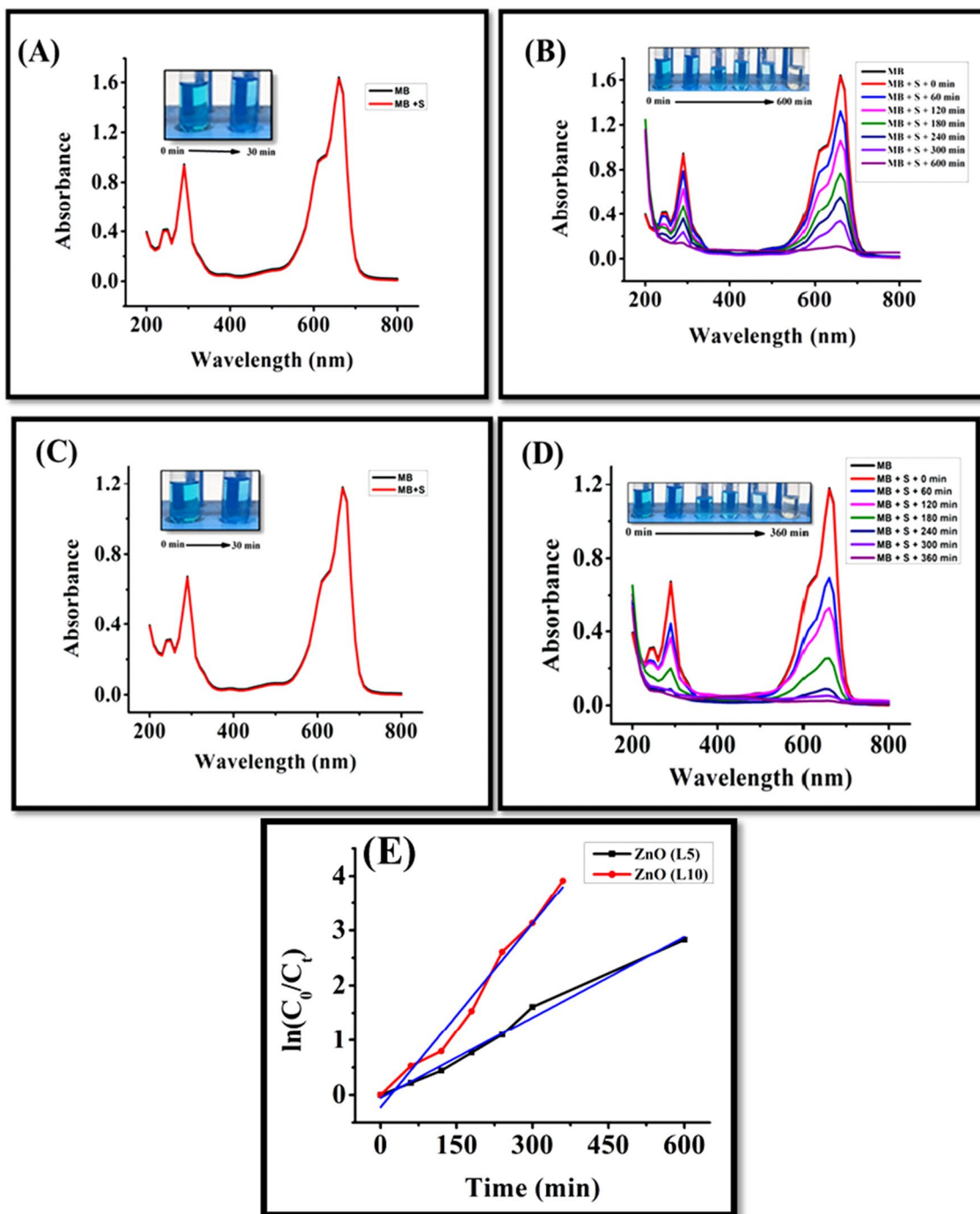
Fig. 7 **A**, **C** UV–Visible spectra of MB dye samples in absence of photocatalysts after 30 min of sunlight irradiation, UV–visible spectra of MB dye samples in presence of (**B**) ZnO (L5) nanoparticles, and (**D**) ZnO (L10) nanoparticles (**E**) Plot of ln(C_0/C_t) vs time (min)

reduction in band gap occurs due to surface defects in Mn-doped ZnO nanoparticles which ultimately lead to enhanced photocatalytic activity for the degradation of organic dyes under visible light irradiation [42]. The other crucial point for the enhanced photocatalytic activity of ZnO (L10) than ZnO (L5) is its small particle size and large surface area of synthesized nanoparticles. The reduction in particle size is responsible for the increased surface area for the adsorption of the dye molecules which is further responsible for the increased photocatalytic activity [9, 38]. Saleh and Djaja have reported that a reduction in average crystallite size and band gap could be responsible

Table 3 Comparison of present study with earlier reported studies

SNO	Photo catalyst	Synthesis techniques	Light source of irradiation / time of light exposure	Organic dye / dye degradation efficiency %	References
1	ZnO/CuO nanocomposite	Hydrothermal technique	Mercury vapor lamp (125W)/100 min	RhB/96.84%	11
2	ZnO/MnV$_2$O$_6$ heterojunction	Facile hydrothermal technique	UV light/60 min	MB/95.2%	2
3	ZnO/MnV$_2$O$_6$ heterojunction	Facile hydrothermal technique	UV light/90 min	MO/91.8%	2
4	TiO$_2$/ZnO heterojunction	Electrospinning technique	Sunlight/120 min	MB/25%	5
5	ZnO nanoparticles	Biosynthesis technique	Sunlight/300 min	MB/90%	17
6	rGO/ZnO nanoparticles	Hydrothermal technique	Visible light/120 min	RhB/97%	9
7	5%Fe/ZnO nanomaterial	Co-precipitation technique	Hg-vapor lamp/100 min	MB/96.70%	16
8	ZnO (L5) nanoparticles	Biosynthesis technique	Sunlight /600 min	MB/94.09%	This work
9	ZnO (L10) nanoparticles	Biosynthesis technique	Sunlight /360 min	MB/97.92%	This work
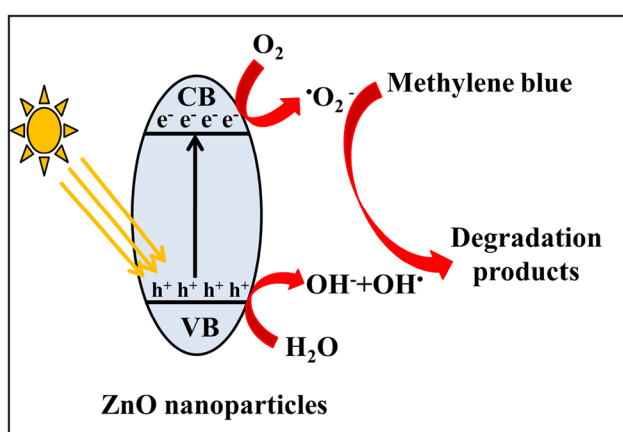
Fig. 8 Schematic diagram of mechanism of photo degradation of MB dye in presence of ZnO nanoparticles

for the enhanced photocatalytic activity of the synthesized ZnO nanoparticles for the degradation of toxic organic dyes such as MB [43].

The mechanism responsible for the photocatalytic degradation of toxic organic MB dye using synthesized ZnO nanoparticles involves the generation of electron–hole pairs on the surface of the nanomaterials due to sunlight irradiation. This leads to a reaction in which a hole from the valence band reacts with the water molecule (H_2O) to form hydroxyl ion (OH$^-$) while an electron from the conduction band reacts with the oxygen molecule (O$_2$) to form oxygen free radical (O$_2^{\cdot-}$). This hydroxyl ion (OH$^-$) further reacts with a hole from the valence band to form hydroxyl free radical (OH$^{\cdot}$). Finally, organic toxic dyes are degraded by O$_2^{\cdot-}$ and OH$^{\cdot}$ free radicals. This mechanism has been reported in the literature [34, 38, 44]. Schematic diagram of mechanism of photo degradation of MB dye in presence of ZnO nanoparticles is given in Fig. 8.

4 Conclusion

- In this article, a green approach has been used effectively to synthesize ZnO (L5) and ZnO (L10) nanoparticles using *Madagascar periwinkle* plant's leaf extract. The green approach is safe, efficient, rapid, and environmentally friendly.

- The Powder X-ray diffraction (PXRD) revealed that synthesized ZnO (L5) and ZnO (L10) nanoparticles consist of a typical hexagonal wurtzite phase.

- The SEM, FESEM, and TEM images of ZnO (L5) and ZnO (L10) reveal that ZnO (L5) nanoparticles are composed of nanorods along with nanoflakes and microflakes. The length of nanorods ranges from 500 to 600 nm while the width of nanorods ranges from 60 to 100 nm.

- The atomic % of Zinc and Oxygen was found to be 28.93% and 71.07% respectively in ZnO (L5) nanoparticles while it was found to be 41.49% and 58.51% respectively in ZnO (L10) nanoparticles.

- The FTIR study reveals that phytochemicals from the leaf of the *Madagascar periwinkle* plant are present on the surface of synthesized ZnO (L5) and ZnO (L10) nanoparticles. This further confirms that leaves of the *Madagascar periwinkle* plant act as a good stabilizing agent in the synthesis of ZnO nanoparticles.

- Brunauer–Emmett–Teller (BET) analysis confirmed that the determined surface areas for ZnO (L5) and ZnO (L10) nanoparticles are 10.202 m^2/g, and 38.762 m^2/g respectively.

- The photocatalytic activity was determined against MB dye. Herein, MB dye was degraded (94.09%) in 600 min by ZnO (L5) photocatalyst and (97.92%) in 360 min by ZnO (L10) photocatalyst. It is evident from this report that ZnO (L10) nanoparticles are a better catalyst than the ZnO (L5) nanoparticles. This higher surface area of ZnO (L10) nanoparticles provides more active sites for

MB photodegradation. Therefore, ZnO (L10) showed higher photocatalytic activity than ZnO (L5) nanoparticles against methylene blue organic dye.

- In the future, photocatalysts can be designed by using these ZnO nanoparticles for the degradation of organic molecules in wastewater. We will also modify these nanoparticles to build nanocomposite with carbon materials to increase their photocatalytic activity against diverse organic chemical molecules.

Authors Contributions Conceptualization, methodology, writing-original draft preparation, Akansha Gupta, Sapna Yadav, and Nutan Rani; supervision and editing, Kalpna Gupta and Kalawati Saini.

Data availability Not applicable.

Declarations

Ethics declarations Not applicable.

Ethics approval Not applicable.

Consent to participate All the authors consented to participate in the drafting of this research article.

Consent for publication All of the authors consented to publish this research article.

Conflict of interest The authors declare no conflict of interest.

References

1. Subki NS (2017) Environmental contamination by batik wastewater and the potential application of activated carbon from pineapple waste for wastewater treatment. Ph. D. Thesis, University Sains Malaysia, Kubang Kerian, Kelantan, Malaysia

2. Patel H, Yadav VK, Yadav KK, Choudhary N, Kalasariya H, Alam MM, Gacem A, Amanullah M, Ibrahium HA, Park JW, Park S, Jeon BH (2022) A Recent and Systemic Approach Towards Microbial Biodegradation of Dyes from Textile Industries. Water 14:3163. https://doi.org/10.3390/w14193163

3. Kaushal S, Kurichh P, Singh PP (2021) Novel 3D fower like ZnO/MnV_2O_6 heterojunction as an efficient adsorbent for the removal of imidacloprid and photocatalyst for degradation of organic dyes in waste water. Polyhedron 201:115161. https://doi.org/10.1016/j.poly.2021.115161

4. Zhang X, Yin Y, Sun Z, Du Y, Ma S, Wu Y (2016) Cr/S/TiO_2-loaded hollow glass microspheres as an efficient and recyclable catalyst for the photocatalytic degradation of indigo carmine under visible light. Quim. Nova 39:956−961. https://doi.org/10.21577/0100-4042.20160121

5. Gao Y, Wang T (2021) Preparation of Ag_2O/TiO_2 nanocomposites by two-step method and study of its degradation of RhB. J Mol Struct 1224:129049. https://doi.org/10.1016/j.molstruc.2020.129049

6. Mousa HM, Alenezi JF, Mohamed IMA, Yasin AS, Hashem AFM, Abdal-hay A (2021) Synthesis of TiO_2@ZnO heterojunction for dye photodegradation and wastewater treatment. J Alloys Compd 886:161169. https://doi.org/10.1016/j.jallcom.2021.161169

7. Wu Y, Pang H, Liu Y, Wang X, Yu S, Fu D, Chen J, Wang X (2019) Environmental remediation of heavy metal ions by novel-nanomaterials: A review. Environ Pollut 246:608–620. https://doi.org/10.1016/j.envpol.2018.12.076

8. Ghanbari F, Zirrahi F, Lin KYA, Kakavandi B, Hassani A (2020) Enhanced electro-peroxone using ultrasound irradiation for the degradation of organic compounds: a comparative study. J Environ Chem Eng 8:104167. https://doi.org/10.1016/j.jece.2020.104167

9. Yadav S, Rani N, Saini K (2022) A review on transition metal oxides based nanocomposites, their synthesis techniques, diferent morphologies and potential applications. IOP Conf Ser: Mater Sci Eng. 1225:012004. https://doi.org/10.1088/1757-899X/1225/1/012004

10. Flilissa A, Laouameur K, HammoudI NE, Tamam N, Yadav KK, Achouri B, Alyami AY, Flilissa O, Algethami JS, Abbasj M, Jeon BH, Benboudiaf S, Benguerba Y (2024) Bentonite SDBS-loaded composite for methylene blue removal from wastewater: An experimental and theoretical investigation. Environ Res 241:117544. https://doi.org/10.1016/j.envres.2023.117544

11. Utami M, Wang S, Musawwa MM, Purbaningtias TE, Fitri M, Yuspita I, Abd-Elkader OH, Yadav KK, Ramanujam GM, Bang D, Chang SW, Ravindran B (2023) Simultaneous photocatalytic removal of organic dye and heavy metal from textile wastewater over N-doped TiO_2 on reduced graphene oxide. Chemosphere 332:138882. https://doi.org/10.1016/j.chemosphere.2023.138882

12. Yadav VK, Yadav KK, Gacem A, Gnanamoorthy G, Ali IH, Khan SH, Jeon BH, Kamyab H, Inwati GK, Choudhary N, Islam S, Cabral-Pinto MMS (2022) A novel approach for the synthesis of vaterite and calcite from incense sticks ash waste and their potential for remediation of dyes from aqueous solution. Sustain Chem Pharm 29:100756. https://doi.org/10.1016/j.scp.2022.100756

13. Naik HS, Sah PM, Dhangade M, Lakkakula J, Raut RW, Roy A, Alghamdi S, Qusty N, Alhindi Z, Kabrah A, Rani A (2023) Synthesis of a silica matrix with ZnO nanoparticles for the fabrication of a recyclable photodegradation system to eliminate methylene blue dye. Green Process Synth 12:20230157. https://doi.org/10.1515/gps-2023-0157

14. Fetimi A, Merouani S, Khan MS, Asghar MN, Yadav KK, Jeon BH, Hamachi M, Senhadji OK, Benguerba Y (2022) Modeling of Textile Dye Removal from Wastewater Using Innovative Oxidation Technologies (Fe(II)/Chlorine and H_2O_2/Periodate Processes): Artificial Neural Network-Particle Swarm Optimization Hybrid Model. ACS Omega 7:13818–13825. https://doi.org/10.1021/acsomega.2c00074

15. Singhal N, Selvaraj S, Sivalingam Y, Venugopal G (2022) Study of photocatalytic degradation efficiency of rGO/ZnO nano-photocatalyst and their performance analysis using scanning Kelvin probe. J Environ Chem Eng 10:107293. https://doi.org/10.1016/j.jece.2022.107293

16. Karim AV, Aydin Hassani A, Eghbali P, Nidheesh PV (2022) Nano-structured modified layered double hydroxides (LDHs)-based catalysts: a review on synthesis, characterization, and applications in water remediation by advanced oxidation processes. Curr Opin Solid State Mater Sci 26:100965. https://doi.org/10.1016/j.ossms.2021.100965

17. Kumari V, Yadav S, Jindal J, Sharma S, Kumari K, Kumar N (2020) Synthesis and characterization of heterogeneous ZnO/CuO hierarchical nanostructures for photocatalytic degradation

of organic pollutant. Adv Powder Technol. 31:2658–2668. https://doi.org/10.1016/j.apt.2020.04.033

18. Giannakis S, Rtimi S, Pulgarin C (2017) Light-assisted advanced oxidation processes for the elimination of chemical and microbiological pollution of wastewaters in developed and developing countries. Molecules 22:1070. https://doi.org/10.3390/molecules22071070

19. Aminuzzaman M, Chong CY, Goh WS, Phang YK, Hock TL, Chee SY, Akhtaruzzaman M, Ogawa S, Watanabe A (2021) Biosynthesis of NiO Nanoparticles Using Soursop (*Annona muricata L.*) Fruit Peel Green Waste and Their Photocatalytic Performance on Crystal Violet Dye. J Clust Sci 32:949–958. https://doi.org/10.1007/s10876-020-01859-8

20. Pandit C, Roy A, Ghotekar S, Khusro A, Islam MN, Emran TB, Lam SE, Khandaker MU, Bradley DA (2022) Biological agents for synthesis of nanoparticles and their applications. J King Saud Univ Sci 34:101869. https://doi.org/10.1016/j.jksus.2022.101869

21. Noor F, Mahmood A, Zafar N, Sarfraz RM, Rehman U, Ijaz H, Hussain Z, Ahmed IA, Imam MT, Abdulmonem WA, Yadav KK, Benguerba Y (2023) Fabrication of pH-responsive hydrogels of perindopril erbumine using black seed extract and β-cyclodextrin co-polymerized with methacrylic acid and methylene bisacrylamide. J Drug Deliv Sci Techno 88:104924. https://doi.org/10.1016/j.jddst.2023.104924

22. Idris DS, Roy A (2024) Biogenic Synthesis of Ag–CuO Nanoparticles and Its Antibacterial, Antioxidant, and Catalytic Activity. J Inorg Organomet Polym Mater 34:1055–1067. https://doi.org/10.1007/s10904-023-02873-9

23. Bhusal U, Roy A, Kunwar S (20230 Bio-fabrication of Cu/Fe/Zn nanoparticles and its antioxidant and catalytic activity. Chem Pap. 77:7099–7111. https://doi.org/10.1007/s11696-023-03001-0

24. Idris DS, Roy A, Subramanian A, Alghamdi S, Chidamabaram K, Qusty NF (2023) Bio-fabrication of Silver-Zinc Bimetallic Nanoparticles and Its Antibacterial and Dye Degradation Activity. J Inorg Organomet Polym Mater. https://doi.org/10.1007/s10904-023-02936-x

25. Di T, Xu Q, Ho W, Tang H, Xiang Q, Yu J (2019) Review on Metal Sulphide-based Z-scheme Photocatalysts. Chem Cat Chem 11:1394–1411. https://doi.org/10.1002/cctc.201802024

26. Mills A, Davies R, H, Worsley D, (1993) Water purification by semiconductor photocatalysis. Chem Soc Rev 22:417–425. https://doi.org/10.1039/CS9932200417

27. Waghchaure RH, Adole VA, Jagdale BS, Koli PB (2022) Fe3+ modifed zinc oxide nanomaterial as an efficient, multifaceted material for photocatalytic degradation of MB dye and ethanol gas sensor as part of environmental rectifcation. Inorg Chem Commun 140:109450. https://doi.org/10.1016/j.inoche.2022.109450

28. Golmohammadi M, Honarmand M, Ghanbari S (2020) A green approach to synthesis of ZnO nanoparticles using jujube fruit extract and their application in photocatalytic degradation of organic dyes. Spectrochim Acta A Mol Biomol Spectrosc 229:117961. https://doi.org/10.1016/j.saa.2019.117961

29. Wetchakun K, Wetchakun N, Sakulsermsuk S (2019) An overview of solar/visible light-driven heterogeneous photocatalysis for water purification: TiO$_2$- and ZnO-based photocatalysts used in suspension photoreactors. J Ind Eng Chem 71:19–49. https://doi.org/10.1016/j.jiec.2018.11.025

30. Gu X, Li C, Yuan S, Ma M, Qiang Y, Zhu J (2016) ZnO based heterojunctions and their application in environmental photocatalysis. Nanotechnology 27:402001. https://doi.org/10.1088/0957-4484/27/40/402001

31. Modi S, Yadav VK, Gacem A, Ali IH, Dave D, Khan SH, Yadav KK, Rather S, Ahn Y, Son CT, Jeon BH (2022) Recent and Emerging Trends in Remediation of Methylene Blue Dye from Wastewater by Using Zinc Oxide Nanoparticles. Water 14:1749. https://doi.org/10.3390/w14111749

32. Pham HNT, Vuong QV, Bowyer MC, Scarlett CJ (2020) Phytochemicals Derived from *Catharanthus roseus* and Their Health Benefits. Technologies 8(4):80. https://doi.org/10.3390/technologies8040080

33. Yadav S, Rani N, Saini K (2022) Green synthesis of ZnO and CuO NPs using Ficus benghalensis leaf extract and their comparative study for electrode materials for high performance supercapacitor application. Mater Today: Proc. 49:2124–2130. https://doi.org/10.1016/j.matpr.2021.08.323

34. Rahman QI, Ahmad M, Misra SK, Lohani M (2013) Efective photocatalytic degradation of rhodamine B dye by ZnO nanoparticles. Mater Lett 91:170–174. https://doi.org/10.1016/j.matlet.2012.09.044

35. Su NR, Lv P, Li M, Zhang X, Li M, Niu J (2014) Fabrication of MgFe$_2$O$_4$-ZnO heterojunction photocatalysts for application of organic pollutants. Mater Lett 122:201–204. https://doi.org/10.1016/j.matlet.2013.12.106

36. Li JF, Rupa EJ, Hurh J, Huo Y, Chen L, Han Y, Ahn JC, Park JK, Lee HA, Mathiyalagan R, Yang DC (2019) *Cordyceps militaris* fungus mediated zinc oxide nanoparticles for the photocatalytic degradation of Methylene blue dye. Optik 183(691):697. https://doi.org/10.1016/j.ijleo.2019.02.081

37. Mahajan P, Singh A, Arya S (2020) Improved performance of solution processed organic solar cells with an additive layer of sol-gel synthesized ZnO/CuO core/shell nanoparticles. J Alloys Compd 814:152292. https://doi.org/10.1016/j.jallcom.2019.152292

38. Yadav S, Yadav J, Kumar M, Saini K (2022) Synthesis and characterization of nickel oxide/cobalt oxide nanocomposite for effective degradation of methylene blue and their comparative electrochemical study as electrode material for supercapacitor application. Int J Hydrog Energy 47:41684–41697. https://doi.org/10.1016/j.ijhydene.2022.02.011

39. Yadav S, Rani N, Saini K (2023) Coupling ZnO with CuO for efcient organic pollutant removal. Environ Sci Pollut Res 30:71984–72008. https://doi.org/10.1007/s11356-022-24139-6

40. Rani N, Yadav S, Mushtaq A, Rani S, Saini M, Rawat S, Gupta K, Saini K, Maity D (2024) Azadirachta indica peel extract-mediated synthesis of ZnO nanoparticles for antimicrobial, supercapacitor and photocatalytic applications. Chem Pap. https://doi.org/10.1007/s11696-024-03340-6

41. Miri A, Vahed HOS, Sarani M (2018) Biosynthesis of silver nanoparticles and their role in photocatalytic degradation of methylene blue dye. Res Chem Intermed. 44:6907–6915. https://doi.org/10.1007/s11164-018-3529-3

42. Ullah R, Dutta J (2008) Photocatalytic degradation of organic dyes with manganese-doped ZnO nanoparticles. J. Hazard. Mater. 156:194–200. https://doi.org/10.1016/j.jhazmat.2007.12.033

43. Saleh R, Djaja NF (2014) UV light photocatalytic degradation of organic dyes with Fe-doped ZnO nanoparticles. Superlattices Microstruct. 74:217–233. https://doi.org/10.1016/j.spmi.2014.06.013

44. Devi LV, Sellaiyan S, Selvalakshmi T, Zhang HJ, Uedono A, Sivaji K, Sankar S (2017) Synthesis, defect characterization and photocatalytic degradation efficiency of Tb doped CuO nanoparticles. Adv Powder Technol. 28:3026–3038. https://doi.org/10.1016/j.apt.2017.09.013